ACS OMEGA

Article

Cite This: ACS Omega 2019, 4, 5795−5804

http://pubs.acs.org/journal/acsodf

# Effect of the Electronic State of Cu, Ag, and Au on Diesel Soot Abatement: Performance of Cu/ZnO, Ag/ZnO, and Au/ZnO Catalysts

Grisel Corro,*[,†] Juan Angel Flores,[†] Francisco Pacheco-Aguirre,[‡] Umapada Pal,[§] Fortino Bañuelos,[†] Rosalía Torralba,[†] and Octavio Olivares-Xometl[‡]

[†]Instituto de Ciencias, Benemérita Universidad Autónoma de Puebla, 4 sur 104, 72000 Puebla, Mexico

[‡]Facultad de Ingeniería Química, Benemérita Universidad Autónoma de Puebla, 72570 Puebla, Mexico

[§]Instituto de Física, Benemérita Universidad Autónoma de Puebla, Apdo. Postal J-48, 72570 Puebla, Mexico

Supporting Information

**ABSTRACT:** Noble metals such as Au, Ag, and Cu supported over semiconducting ZnO are well-known heterogeneous oxidation catalysts. All of them have been utilized for the oxidation of diesel soot with varied success. However, Au-supported ZnO is seen to be superior among them. Here, we present a comparative study of all these three catalysts for diesel soot oxidation to explain why Au/ZnO is the best among them, demonstrating the contribution of electronic states of metals in composite catalysts. The electronic states of Cu, Ag, and Au determined by X-ray photoelectron spectroscopy on 1 wt % Cu/ZnO, 1 wt % Ag/ZnO, and 1 wt % Au/ZnO catalysts were correlated with their diesel soot oxidation activities. Although all three catalysts present reasonable diesel soot oxidation activities at relatively low temperature, 1% Cu/ZnO and 1% Ag/ZnO oxidize only about 60% of the deposited diesel soot around 250 °C and 1% Au/ZnO oxidizes 100% of the deposited diesel soot, at a temperature as low as 230 °C. The activity of the catalysts is attributed to the formation of stable $M^0-M^{\delta+}$ bifunctional catalytic sites at the metal−ZnO interface, which enhances the contact efficiency of solid diesel soot on $M^{\delta+}$ and generates the superoxide species on $M^0$ moieties. The stability of the bifunctional $M^0-M^{\delta+}$ sites is controlled by the electronic interactions between the metal (M) and n-type semiconductor ZnO at their interface. Very high activity of 1% Au/ZnO is attributed to the presence of $Au^{3+}$ at the catalyst surface, which generates a stronger Coulombic force with diesel soot electrons. We demonstrate a direct relation between the diesel soot oxidation activity of these three metals and their electronic states at the catalyst surface.

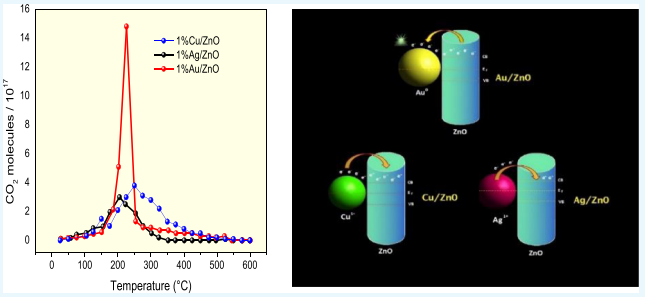


## 1. INTRODUCTION

There is an increased demand of diesel-powered vehicles in recent years, owing to their efficient energy conversion, higher durability, and operation reliability, compared to gasoline-powered vehicles.[1] However, emission of diesel soot from diesel engines causes severe environmental and health problems to humans, animals, and plants. The increasingly stringent U.S. and European emission standards demand a drastic reduction in the emission of nitrogen oxides and soot from diesel engines, which requires technical improvements in the current diesel engines along with improved after-treatment technologies.

One of the most effective after-treatment technologies for diesel soot control is based on a diesel soot filter, in which particles are trapped.[2] The filter has to be regenerated periodically by the combustion of trapped soot. However, the direct oxidation of soot requires higher temperatures (around 600 °C) than the highest diesel engine exhaust gas temperature, which is around 400 °C for most of the diesel engines.[3] Such a high temperature in the filter is generally attained by injecting a diesel fuel into the exhaust, which results in additional fuel consumption and thermal stress to the filter.

A catalyzed diesel soot filter is regarded as the best solution to reduce the soot emissions from diesel engines. In these filters, soot is trapped and simultaneously oxidized at exhaust gas temperatures (~400 °C).[4] However, catalytic soot oxidation is quite slow because of the large size of the soot particles, which hardly diffuse into the catalyst micropores or mesopores. Thus, the contact between the catalyst surface and the soot particles is very low.[5] An interesting solution to this problem is the continuously regenerating trap (CRT), in which the soot oxidation occurs at relatively lower temperatures.[8] In this technology, NO is first oxidized to $NO_2$ over a platinum catalyst. $NO_2$ functions as a mobile species, creating a catalyst−soot contact and lowering the soot oxidation temperature. However, the use of CRT is severely restricted

Received: November 10, 2018
Accepted: January 22, 2019
Published: March 25, 2019






DOI: 10.1021/acsomega.8b03142
ACS Omega 2019, 4, 5795−5804

because of the restriction imposed by diesel engine emission norms, which demands a strong decrease of $NO_x$ emissions.

On the other hand, organometallic fuel additives known as fuel-borne catalysts (FBCs) can lower the soot oxidation temperature in soot filters. In this technology, a catalyst-doped soot is formed during combustion in diesel engines. However, the application of this technology is strongly restricted because while the diesel soot oxidation temperature is lowered, the FBCs are consumed continuously and the catalysts (metal oxides) are accumulated as ash inside the filter.[6,7]

Some of the catalysts that show good catalytic performances in diesel soot oxidation are based on a variety of active materials such as transition metals, transition-metal oxides, alkaline metal oxides, perovskites, rare earth oxides, and a mixture of two or more of them.[9−13] One of the main catalytic functions of transition metals in oxidation reactions is to transfer the oxygen species from their surface to the reactants.[14] Therefore, the activity of these catalysts for oxidizing soot particles is the function of their ability to activate oxygen and the contact probability between the catalyst and the soot particles.[15,18] In other words, these catalysts must contain active sites for adsorbing and activating $O_2$ along with active sites for adsorbing diesel soot to generate close contacts.[16,17]

In recent studies, we have reported the diesel soot oxidation activity of group IB metals such as Cu/ZnO, Ag/ZnO, and Au/ZnO deposited over ZnO.[19−21] The activity of diesel soot oxidation is seen to vary drastically from one catalyst to the other. While Cu/ZnO and Ag/ZnO present low activity for diesel soot oxidation, Au/ZnO is seen to be very active for this reaction at temperatures as low as 230 °C. The unique fact common for all these three catalysts, noticed through their X-ray photoelectron spectroscopy (XPS) analysis, is the presence of both metallic and ionic species at their surfaces. The results of diesel soot oxidation study of the three catalysts suggest that the catalytic reactions over them strongly depend on the electronic states of the supported metals (Cu, Ag, and Au). The difference in their electronic states is governed through the differences in the electronic interactions of the metallic nanoparticles (NPs) with ZnO at their interfaces. In this work, we present a comparative study, unifying diesel soot oxidation results of all three catalysts, to demonstrate how the electronic states of these noble metals control the diesel soot oxidation behavior of metal−semiconductor nanocomposites. The origin of different electronic states of the metals at the support surface has been explained by considering their electronic interactions with the support ZnO, which is an n-type wide band gap semiconductor.

## 2. RESULTS AND DISCUSSION

**2.1. Diesel Soot Characterization.** Fourier transform infrared (FT-IR) absorption spectrum of the diesel soot studied in this investigation is presented in Figure 1. The spectrum revealed characteristic absorption peaks in the mid-infrared region. The characteristic signals of C−H symmetric and asymmetric stretching vibrations of alkane and alkene-type functional groups appeared at around 2950, 2920, and 2854 $cm^{-1}$, respectively. The peak detected at around 1711 $cm^{-1}$ can be assigned to the carbonyl C═O stretching in aromatic and aliphatic aldehydes and ketones. The absorption band appeared around 1548 $cm^{-1}$ could be attributed to C═C stretching of aromatics and alkenes. The absorption band revealed around 1462 $cm^{-1}$ corresponds to conventional

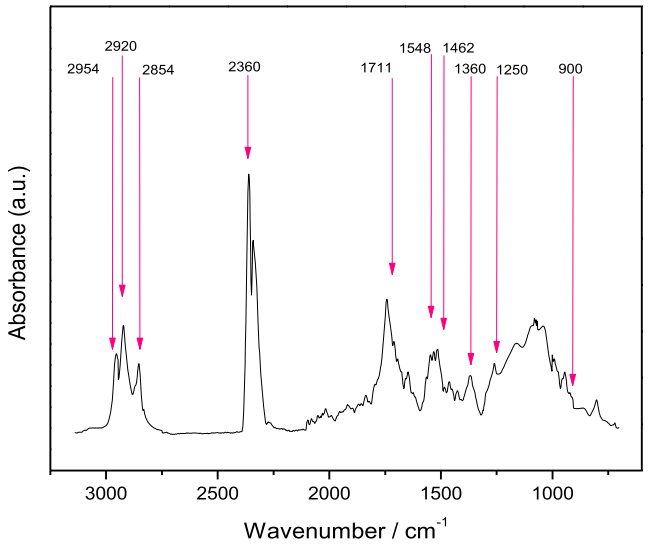


**Figure 1.** FT-IR spectrum of the diesel soot collected on reference ZnO from the combustion vessel exhaust during the burning of diesel fuel.

coke.[22,23] The signal appeared around 1360 $cm^{-1}$ has also been observed in activated carbon, graphite, and carbon black.[24]

The broad signal detected between 1250 and 900 $cm^{-1}$ might be the result of overlapping of the following peaks: C−O stretching (1191 and 1070 $cm^{-1}$), C−O−C stretching (1121 $cm^{-1}$), and C−C−O stretching.[22] The band detected at around 2360 $cm^{-1}$ corresponds to $CO_2$ adsorbed on the catalysts.

**2.2. Catalyst Characterization.** *2.2.1. Surface Area Analysis.* Specific surface areas ($S_g$) of the catalysts were determined from their $N_2$ adsorption−desorption isotherms recorded at 77 K. The results obtained are summarized in Table 1. As can be seen, all the freshly prepared catalysts revealed their very low specific surface area.

**Table 1. Texture Properties of the Freshly Prepared Composite Catalysts**

| catalyst | specific surface area ($m^2\ g^{-1}$) | average size of metal NPs (nm) |
|---|---|---|
| ZnO | 4.52 | |
| 1% Cu/ZnO | 3.31 | 53.0 |
| 1% Ag/ZnO | 3.40 | 88.0 |
| 1% Au/ZnO | 3.93 | 89.3 |

*2.2.2. TEM Characterization of the Catalysts.* Representative transmission electron microscopy (TEM) images of 1% Cu/ZnO, 1% Ag/ZnO, and 1% Au/ZnO catalysts recorded after their use in the diesel soot oxidation cycle are presented in Figures 2 and S1 (Supporting Information). As can be seen, while after use in the diesel soot oxidation cycle, Au and Ag NPs of average (ca.) size ∼90 nm are formed over the ZnO surface, Cu NPs of wide size dispersion (10−140 nm size range) were formed over the support. The average (ca.) size of the Cu NPs was considerably smaller (∼53 nm) than the average size of Au and Ag NPs (Table 1).

In Figure 2, we can also see that both the gold and silver NPs are hemispherical in shape. These NPs are attached to the support through their flatter planes over a specific crystal orientation of the support crystallites. These images suggest



DOI: 10.1021/acsomega.8b03142
ACS Omega 2019, 4, 5795−5804

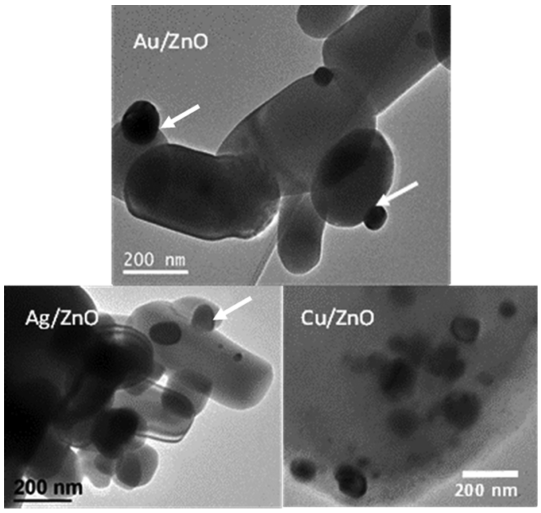


**Figure 2.** Typical TEM images of the 1% Au/ZnO, 1% Ag/ZnO, and 1% Cu/ZnO catalysts.

that the interfaces between Au or Ag NPs and ZnO are in tight contact (shown by white arrows).

*2.2.3. Diffuse Reflectance Spectra of 1% Au/ZnO, 1% Ag/ZnO, and 1% Cu/ZnO Catalysts.* Figure 3 shows the UV−vis diffuse reflectance spectra (DRS) of all the catalysts studied in this investigation. Although the absorption spectrum of ZnO revealed a low absorption in the visible spectral region with a sharp absorption below 400 nm, the absorption in the visible spectral region is high for all the three M/ZnO composites. The broad absorption bands peaked around 450 and 510 nm in the spectra of 1% Ag/ZnO and 1% Au/ZnO samples can be associated with the surface plasmon resonance (SPR) absorption of the Ag and Au NPs formed in the respective composites.[25−27] On the other hand, the absorption spectrum of the 1% Cu/ZnO catalyst revealed a broad absorption signal between 550 and 650 nm, corresponding to the SPR of metallic Cu particles and a broad hump spreading through 400−510 nm associated with the absorption of $Cu^{+}$.[28] In general, the onset of absorption edge for all the composite catalysts remained close to 380 nm (Figure 3), which is close to the absorption edge of the ZnO semiconductor.[29] However, linear fits to the sharp absorption sections of the spectra revealed that their band gap energy differs slightly.

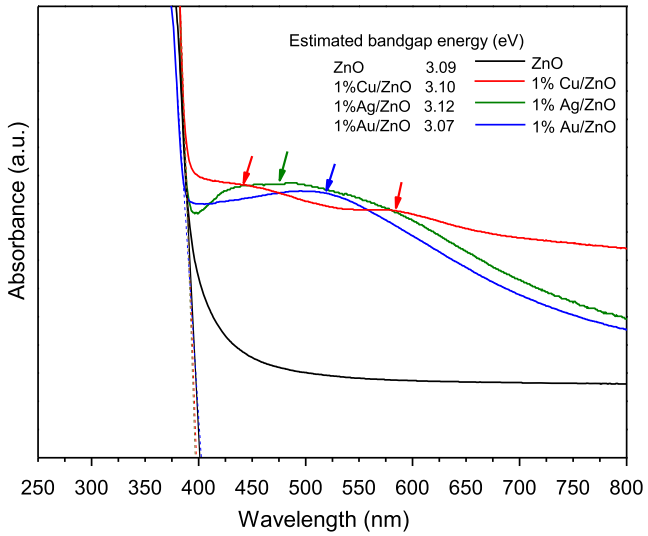


**Figure 3.** UV−vis DRS absorption spectra of ZnO, 1% Cu/ZnO, 1% Ag/ZnO, and 1% Au/ZnO. The band edge positions of the composites are indicated by thick dotted dashed lines and the maxima of the SPR absorption bands are indicated by continuous arrows of respective colors.

As can be noticed, the absorption band of the 1% Ag/ZnO catalyst in the visible spectral range is exceptionally broad, covering almost the whole part of the visible region (400−650 nm) with a maximum at around 450 nm, which might be the result of overlapping the silver surface plasmonic resonance signal with the $\sigma-\sigma^*$ and $n-\sigma^*$ transition signals of $Ag_n$ clusters, which appear in the 330−360 and 440−540 nm spectral range, respectively.[25,26] It is important to indicate that the band at 275 nm attributed to $Ag_4^{2+}$ (produced from the dimerization of $Ag_2^{+}$) cannot be observed because of the overlapping of the broad absorption signals spreading through 200 and 400 nm of ZnO.[30,31]

It is interesting to compare the absorption spectrum of pure ZnO with the spectra of the supported catalysts. As can be observed, the absorption edges of ZnO, 1% Cu/ZnO, 1% Ag/ZnO, and 1% Au/ZnO are not superposed. Although the absorption edge of the 1% Cu/ZnO and 1% Ag/ZnO catalysts suffered a small shift toward lower wavelengths, the band edge of the 1% Au/ZnO catalyst shifted toward higher wavelength.

These small shifts of band edge of the composite catalysts can be explained by considering a probable interfacial electronic interaction between the metals and the semiconductor support. The red shift (toward lower energy) observed for the ZnO absorption edge in the 1% Au/ZnO spectrum might be due to the electronic transfer from ZnO to Au NPs at their interface. The blue shift (toward higher energy) of the band edge detected for 1% Ag/ZnO and 1% Cu/ZnO samples might be caused by the electron transfer occurred from the Ag or Cu NPs to the ZnO support at their interface. Although an increase in electron population in the conduction band (CB) of ZnO effectively increases its band gap due to the Burstein−Moss effect, the opposite can take place due to decrease in electron population at the CB of the semiconductor.[32] These shifts are due to the interfacial electronic interactions between the metals and ZnO. As the interfacial area is a small region at the catalyst surface, the shifts of the band edge are small, as expected. The results presented in Figure 3 also suggest the presence of Cu, Ag, and Au in their ionic and metallic states, which was supported by the results obtained from the XPS analysis of the catalysts, presented in the next section.

*2.2.4. XPS Characterization of 1% Au/ZnO, 1% Ag/ZnO, and 1% Cu/ZnO Catalysts.* The capability of a catalyst to activate oxygen is closely associated with its activity in oxidation reactions. The electronic states of Cu, Ag, and Au supported on ZnO were determined by XPS to determine the possible interactions between the catalysts and oxygen during oxidation reactions. The binding energies (BEs) for the core electrons and estimated metal/Zn atomic ratios of the catalysts are presented in Table 2.

*2.2.4.1. 1% Cu/ZnO Catalyst.* The identification of both $Cu^{+}$ and $Cu^{0}$ copper species in solid catalysts is difficult from XPS analysis alone. The BEs of the Cu $2p_{3/2}$ core-level emissions from $Cu^{+}$ and $Cu^{0}$ are essentially the same and are detected at about 1.4 eV below that of $Cu^{2+}$ ions.[33] Therefore, we analyzed their $L_3VV$ X-ray-induced Auger emissions (AEs)



DOI: 10.1021/acsomega.8b03142
ACS Omega 2019, 4, 5795−5804

**Table 2. BEs of the Components and Surface Metal/Zn Atomic Ratio of the Catalysts**[a]

| catalyst | metal BE (eV) | Zn $2p_{3/2}$ (eV) | atomic ratio metal/Zn |
|---|---|---|---|
| 1% Au/ZnO | Au $4f_{7/2}$ | | |
| | 83.4 (7) | 1021.8 | 0.19 |
| | 85.6 (9) | | |
| | 88.0 (84) | | |
| 1% Ag/ZnO | Ag $3d_{5/2}$ | | |
| | 367.3 (80) | 1021.8 | 0.26 |
| | 368.3 (20) | | |
| 1% Cu/ZnO | Cu $\alpha_A$ | | |
| | 1849.2 (90) | 1020.8 | 0.38 |
| | 1851.0 (10) | | |

[a]The % peak area of the components are presented in parentheses.

to identify $Cu^+$ and $Cu^0$ in the 1% Cu/ZnO catalyst. The Auger parameter ($\alpha_A$) was defined as

$$\alpha_A = h\nu + (\text{BE Cu } 2p_{3/2} - \text{BE Cu}_{L_3VV}) \quad (1)$$

where $h\nu$ is the energy of the incident photon (1253.6 eV), BE Cu $2p_{3/2}$ is the BE of the Cu $2p_{3/2}$ photoelectron, and BE $Cu_{L_3VV}$ is the $L_3VV$ Auger emission.

The $Cu_{L_3VV}$ Auger spectrum of 1% Cu/ZnO is dominated by the $Zn_{L_3VV}$ Auger peaks that appeared in the same energy region as of $Cu_{L_3VV}$. Nevertheless, the peak fitting procedure allowed us to determine the $Cu_{L_3VV}$ contribution. In Figure 4,

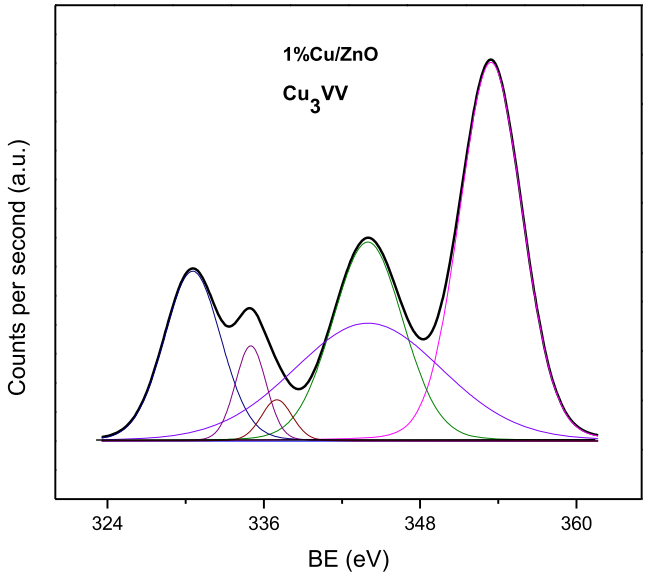


**Figure 4.** $Cu_{L_3VV}$ Auger transition of 1% Cu/ZnO.

the core-level spectrum of the sample is presented. In Table 2, the BEs of Zn $2p_{3/2}$ and Cu $2p_{3/2}$ levels, the values of $\alpha_A$, and the Cu/Zn atomic ratios in the catalyst are presented.

*2.2.4.2. 1% Ag/ZnO Catalyst.* The XPS spectrum of 1% Ag/ZnO is displayed in Figure 5. The XPS estimated that the Ag/Zn atomic ratio (presented in Table 2) is about 0.26. As it has been listed in Table 2, the Ag $3d_{5/2}$ emission band comprises two components. The component located at around 367.3 eV corresponds to $Ag^+$ and the component at 368.3 eV corresponds to $Ag^0$ electronic states.[34−38] Our analysis revealed a high amount of $Ag^+$ at the surface of the catalyst.

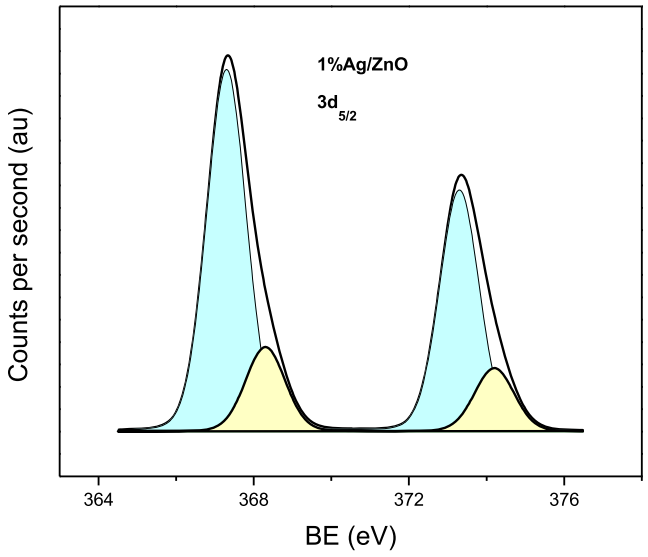


**Figure 5.** XPS spectrum of 1% Ag/ZnO.

However, the catalyst was reduced during its preparation in pure $H_2$ at high temperature, suggesting the presence of $Ag^0$ at the surface of the catalyst. Now, the enthalpy of formation of bulk $Ag_2O$ ($-\Delta H_f$ = 7 kcal/mol) is very low. This value indicates that the surface oxidation of $Ag^0$ to $Ag_2O$ is hardly possible under the present reduction conditions, or even in higher temperatures of oxidation conditions.[39] Notwithstanding, the XPS analysis revealed a high percentage of $Ag^+$ after catalyst reduction.

*2.2.4.3. 1% Au/ZnO Catalyst.* From the XPS analysis results of sample 1% Au/ZnO presented in Figure 6 and Table 2, we

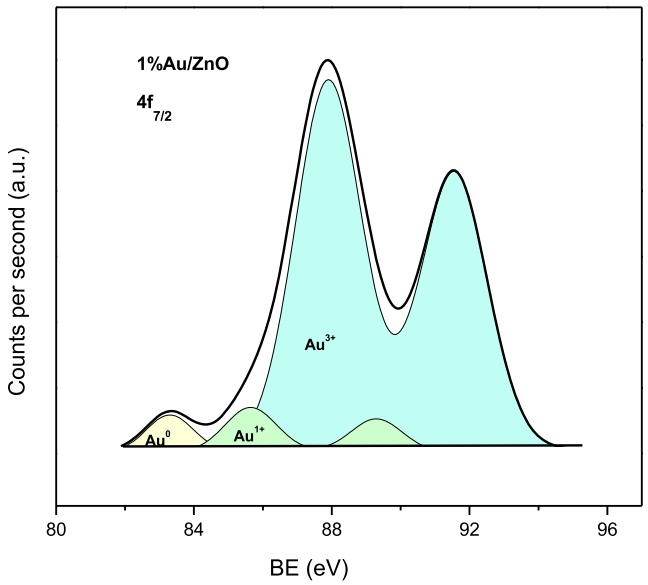


**Figure 6.** XPS spectrum of 1% Au/ZnO.

can see that the XPS spectrum of the catalyst revealed the Au $4f_{7/2}$ emission band with three components. These components are located at around 83.4, 85.6, and 88.0 eV and correspond to $Au^0$, $Au^+$, and $Au^{3+}$ electronic states, respectively. The analysis revealed high amounts of $Au^{3+}$ (84%) with minor contributions of $Au^0$ and $Au^+$. The Au/Zn atomic ratio value at the surface of the catalyst (Table 2) is



DOI: 10.1021/acsomega.8b03142
ACS Omega 2019, 4, 5795−5804

about 0.19 only. This value indicates a low metal dispersion and the formation of gold NPs of high average particle size, supporting the observation made from the TEM micrograph of the sample (Figure 2).

*2.2.5. Metal–Support Interactions in 1% Cu/ZnO, 1% Ag/ZnO, and 1% Au/ZnO Catalysts.* The XPS analysis of electronic states of Cu, Ag, and Au in the catalysts revealed the presence of metallic and ionic species at their surfaces. The presence of these species can be explained by considering the energy level alignment concept, correlating the interactions of Cu, Ag, or Au at the interface with ZnO, which is an n-type semiconductor.

The work function values of ZnO, Au, Ag, and Cu are presented in Table 3. ZnO presents a work function value of

**Table 3. Work Function Values of the Different Compounds in the Catalysts**

| compound | work function (eV) |
|---|---|
| ZnO | 4.9 |
| Cu | 4.6 |
| $Cu^{+}$ | 4.9 |
| $Cu^{2+}$ | 5.9 |
| Ag | 4.2 |
| $Ag^{+}$ | 5.3 |
| Au | 5.1 |
| $Au^{+}$ | |
| $Au^{3+}$ | |

4.9 eV, which is higher than that of metallic Cu (4.6 eV) and metallic Ag (4.26 eV). Because of the energy level alignment, the Fermi level of Cu and Ag remains at higher level than that of ZnO. Therefore, when in contact, the electrons migrate from copper or silver to the CB of ZnO at their interface, to achieve the Fermi level equilibration. The electron migration process causes a reduction in the stability of metallic copper or metallic silver at the metal–support interface.[40,41] As revealed by XPS analysis (Table 2), the formation of $Cu^{+}$ or $Ag^{+}$ results from the electron transfer from metallic Cu or Ag to ZnO at the metal–support interface. As can be observed in Table 3, although about 10% of $Cu^{+}$ was revealed at the 1% Cu/ZnO surface, the presence of about 80% $Ag^{+}$ was revealed at the surface of the 1% Ag/ZnO catalyst. The strong difference between $Cu^{+}$ and $Ag^{+}$ surface concentrations may be due to the work function differences of Cu and Ag (Table 3). Indeed, Ag presenting a lower work function value (4.2 eV) than that of Cu (4.6 eV) has a higher value of its Fermi level energy than that of Cu. The transfer of electrons from Cu to ZnO until the two systems attain equilibrium for the new Fermi level to be established may be lower than the transfer of electrons from Ag to ZnO, resulting in a higher concentration of $Ag^{+}$ compared with the $Cu^{+}$ concentration at the surface of the catalysts.

The work function of Au (5.1 eV) is a bit higher than that of ZnO (4.9 eV). Therefore, the Fermi level of ZnO remains at a bit higher energy than that of gold. In this case, the electrons will migrate from the CB of ZnO to Au at their interface to achieve the Fermi level equilibration when they are in contact. The Fermi level equilibration increases the stability of metallic gold at the Au–ZnO interface.[40,41] The formation of very stable metallic $Au^{0}$ results from the electron transfer from ZnO to Au as revealed by XPS (Table 2).

XPS analysis revealed high amounts of $Au^{3+}$ (84%) with minor contributions of $Au^{0}$ and $Au^{+}$. However, the catalyst was reduced during its preparation in pure $H_2$ at high temperature, justifying the presence of $Au^{0}$ at the surface of the catalyst. Moreover, TEM results revealed the presence of large Au particles at the catalyst surface, which should behave as bulk gold, which is rarely found in oxidized state. Now, as the 1% Au/ZnO catalyst was prepared using $NaAuCl_4$ solution, chloride traces might have remained despite the $H_2$ reduction at 450 °C. The presence of $AuCl_3$ also cannot be discarded, which would be responsible for the $Au^{3+}$ contribution at the catalyst surface. However, at the ZnO–Au interfacial region, the electron transfer from ZnO to Au might have resulted in the formation of metallic Au, despite the interactions between gold and chloride in other regions of the catalyst.

The results obtained from the DRS spectra of the composite catalysts (Figure 2) support these assumptions. The electronic transfer from copper and silver to ZnO might have generated an enrichment of electrons in ZnO support, which might have resulted in the blue shift of its band gap energy. On the other hand, the electron transfer from ZnO to gold might have generated a decrease in the electronic density of interfacial ZnO molecules, resulting in the red shift of its band gap observed in the absorption spectrum of 1% Au/ZnO.

**2.3. Diesel Soot Oxidation on the Catalysts.** Generation of CO during diesel soot oxidation reactions was not detected in the studied soot oxidation conditions of this investigation (25–600 °C, 20 vol % $O_2$), which might be due to the high oxidation activity of 1% Cu/ZnO, 1% Ag/ZnO, and 1% Au/ZnO catalysts. The CO oxidation rate might have been higher than the CO generation rate during soot oxidation over the catalysts. Indeed, these results show that the diesel soot reacts predominantly via the combustion reaction at the very strong oxidation conditions in which the reaction is performed (20 vol % of $O_2$). Nevertheless, the evolutions of diesel soot oxidation over ZnO at 25–800 °C revealed only trace amounts of CO at about 500 °C.

The $CO_2$ evolutions during the diesel soot oxidation with temperature over the three catalysts studied are displayed in Figure 7. From these curves, the $T_{initial}$ (temperatures at which the oxidation started), $T_{max}$ (temperatures when the oxidation reached a maximum), and $T_{final}$ (temperatures when the

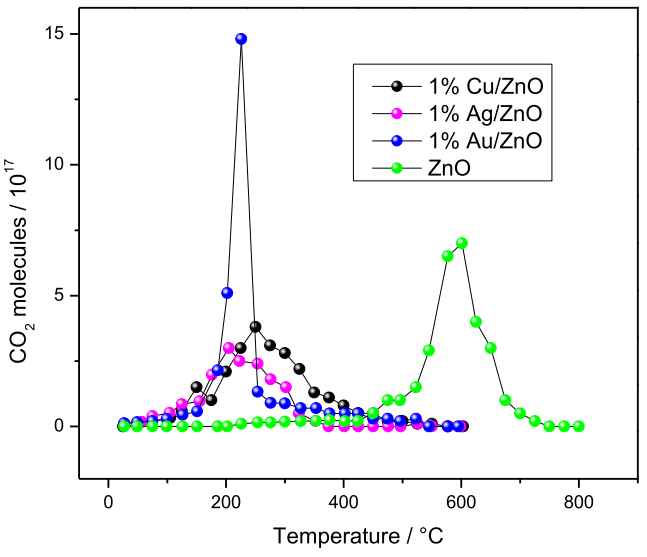


**Figure 7.** Evolution of $CO_2$ as a function of temperature during diesel soot oxidation over the catalysts.



DOI: 10.1021/acsomega.8b03142
ACS Omega 2019, 4, 5795–5804

Table 4. Integrated Areas under $CO_2$ Evolution ($[CO_2]_{Cat}$), $[CO_2]_{Cat}/[CO_2]_{ZnO}$ Ratios, and $T_{initial}$, $T_{max}$, and $T_{final}$ for the Catalysts During the Diesel Soot Oxidation

| catalyst | $[CO_2]_{Cat}$ ($10^{18}$ molecules °C) | $[CO_2]_{Cat}/[CO_2]_{ZnO}$ | $T_{initial}$ | $T_{max}$ | $T_{final}$ |
|---|---|---|---|---|---|
| | | | temperatures (°C) | | |
| ZnO | 845[a] | 1.00 | 225 | >600 | >600 |
| 1% Cu/ZnO | 634 | 0.74 | 100 | 250 | 450 |
| 1% Ag/ZnO | 542 | 0.63 | 75 | 205 | 325 |
| 1% Au/ZnO | 841 | 0.99 | 95 | 225 | 450 |

[a]Calculated from 25 to 800 °C.

reaction completed) were calculated for the three catalysts and presented in Table 4. As can be noticed from Figure 7 and Table 4, the diesel soot oxidation activity of all the three catalysts takes place at temperatures <400 °C.

In Figure 7, $CO_2$ evolution during diesel soot oxidation deposited over reference ZnO in between 25 and 800 °C is presented. In these reaction conditions, the total area under the $CO_2$ evolution curve from 25 to 800 °C ($[CO_2]_{ZnO}$) was used as a measurement of the highest amount of carbon in the diesel soot, which was accumulated over the catalysts for 1 h. To compare the catalytic activity of our three catalysts, the areas under the $CO_2$ evolution curves, during the diesel soot oxidation over the catalysts ($[CO_2]_{Cat}$), were estimated and compared with $[CO_2]_{ZnO}$. The calculated values of $[CO_2]_{Cat}$ and $[CO_2]_{Cat}/[CO_2]_{ZnO}$ are reported in Table 4. In the table, it can be seen that $[CO_2]_{Au}/[CO_2]_{ZnO}$ (calculated for 1% Au/ZnO) attained the highest value compared with the calculated values for 1% Cu/ZnO and 1% Ag/ZnO. These results indicate that 1% Au/ZnO is a very active and superior catalyst for diesel soot oxidation. The appearance of intense and sharp signal (Figure 7) in 200−300 °C temperature range, with a peak at 230 °C, indicates that the diesel soot deposited during diesel combustion is probably fully oxidized at this low temperature.

*2.3.1. Mechanistic Considerations of Diesel Soot Oxidation over the Catalysts.* The differences in the activities presented by 1% Cu/ZnO, 1% Ag/ZnO, and 1% Au/ZnO for diesel soot oxidation cannot be explained by the estimated specific surface area of the catalysts. As can be seen in Table 1, all the three catalysts present a similar specific surface area. On the other hand, the diesel soot oxidation activities of the catalysts (Figure 7 and Table 4) cannot be explained neither by the differences in the average metal NP size in them. Although the TEM images of 1% Ag/ZnO and 1% Au/ZnO (Figure 2) revealed the formation of metal NPs of very similar (~88 nm for Ag and 89 nm for Au) average sizes in the composite catalysts, the gold-supported catalyst manifests much higher diesel soot oxidation activity. On the other hand, the 1% Cu/ZnO catalyst, containing metallic NPs of about 53 nm average size, presents the same behavior as 1% Ag/ZnO catalyst.

The catalytic behavior of the three catalysts cannot be explained by the metal surface atomic concentration revealed by XPS (Table 2). It can be seen that the relative atomic ratio (M/Zn) decreases in the order: Cu > Ag > Au. However, the $[CO_2]_{Cat}/[CO_2]_{ZnO}$ ratio shown in Table 4 decreases in the order: Au > Cu > Ag.

Therefore, to explain the exceptionally high diesel soot oxidation activity of 1% Au/ZnO at low temperature in comparison to 1% Cu/ZnO and 1% Ag/ZnO, it is convenient to explain first the effects of 1% Au/ZnO on the oxidation reaction. On the basis of the results of XPS analysis of the catalyst surface, we propose a bifunctional catalytic site consisting of neighboring $Au^0$ and $Au^{3+}$ ($Au^0$−$Au^{3+}$). The $Au^0$ sites may be located at the Au/ZnO interface and the $Au^{3+}$ site at the gold NP surface, in close proximity to $Au^0$ (Figure 8). This site might have facilitated the diesel soot oxidation following a Langmuir−Hinshelwood reaction mechanism, according to the following steps:

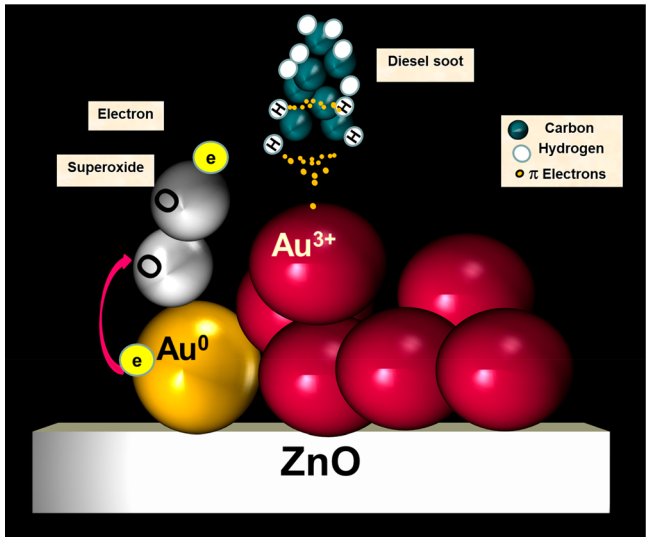


**Figure 8.** Proposed catalytic site model at the Au/ZnO surface.

*2.3.1.1. First Step.* At the Au/ZnO interface, $O_2$ was adsorbed on the $Au^0$ moiety of the catalytic site ($Au^0$−$Au^{3+}$) and superoxide ions ($O_2^-$) were generated. Superoxide species are very active species for optimizing the oxidation of diesel soot.[42−47]

*2.3.1.2. Second Step.* The second step involves simultaneous adsorption of diesel soot at the $Au^{3+}$ moiety of the catalytic site. The probability of the diesel soot adsorption occurrence on the catalyst surface will increase with the number of activated diesel soot molecules striking the surface. The striking molecules, to be adsorbed, must carry a total energy equal to or greater than the adsorption activation energy. The total energy $E_T$ of the diesel soot particle is considered to be the sum of its kinetic energy $E_K$ (defined by the kinetic theory of gases) plus its potential energy $U_C$ (generated by the Coulombic forces between the $\pi$ electrons of the C=C bonds present in the diesel soot molecules and the $Au^{3+}$ moiety of the catalytic site), according to the following equation:

$$E_T = E_K + U_C \quad (2)$$

The total energy of the diesel soot particles being adsorbed at the $Au^{3+}$ moiety can be expressed as



DOI: 10.1021/acsomega.8b03142
ACS Omega 2019, 4, 5795−5804

$$E_{T\,Au} = \frac{3}{2}k_B T + 3k_c\frac{e^2}{r} \quad (3)$$

where $k_B$ is the Boltzmann constant, $T$ is the absolute temperature, 3 stands for the charge number (oxidation state) of $Au^{3+}$, $k_c$ is the Coulomb constant, $e$ is the electric charge, and $r$ is the distance between the charges.

*2.3.1.3. Third Step.* Reaction of the H−C bond of the adsorbed diesel soot molecule at the $Au^{3+}$ moiety with the superoxide formed at $Au^0$. This step may result in the abstraction of H atoms by the very active superoxide ions. The reaction between the superoxides formed over $Au^0$ with the adsorbed diesel soot at $Au^{3+}$ would strongly increase the rate of diesel soot oxidation. The successive, simultaneous interactions of H−C bonds of the diesel soot molecule with $O_2^-$ at the catalyst surface may result in the generation of $CO_2$ and $H_2O$ molecules (as the final products) at low oxidation temperature.

For 1% Cu/ZnO and 1% Ag/ZnO, based on their XPS analysis, we propose a similar catalytic site model at the catalyst surface (Figures 9 and 10), involving $Cu^+$ or $Ag^+$ at the

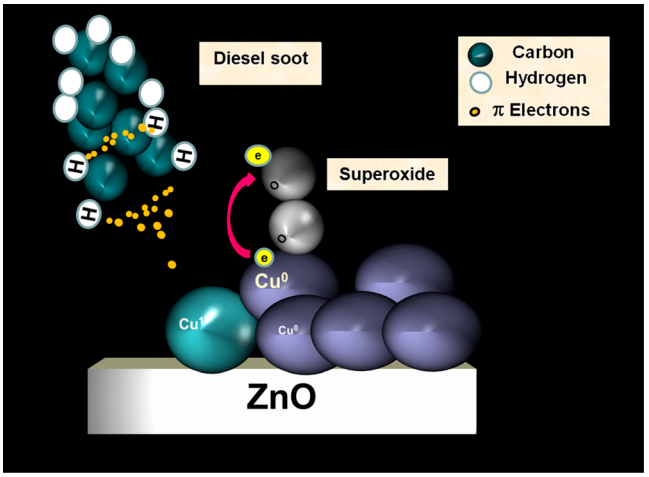


**Figure 9.** Proposed catalytic site model at the Cu/ZnO surface.

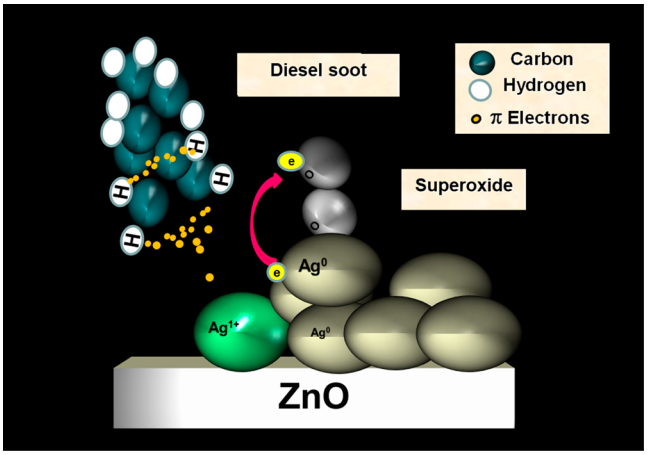


**Figure 10.** Proposed catalytic site model at the Ag/ZnO surface.

Cu/ZnO or Ag/ZnO interfaces, and surface $Cu^0$ or $Ag^0$ sites in proximity to $Cu^+$ or $Ag^+$. Developed bifunctional catalytic sites consisting of $[Cu^+-Cu^0]$ or $[Ag^+-Ag^0]$ would facilitate the particle matter oxidation following a similar mechanism at the bifunctional $[Au^0-Au^{3+}]$ site.

However, the adsorption rate of diesel soot at the $Cu^+$ or $Ag^+$ moieties of the proposed catalytic sites (step 2) would be much lower than the adsorption rate at the $Au^{3+}$ moieties of the catalytic sites of 1% Au/ZnO. To provide a mathematical justification of such assumption, we calculated the total energy $E_T$ value of each diesel soot molecule striking the catalytic sites of copper or silver catalysts:

$$E_{T\,Cu} = \frac{3}{2}k_B T + 1k_c\frac{e^2}{r} \quad (4)$$

$$E_{T\,Ag} = \frac{3}{2}k_B T + 1k_c\frac{e^2}{r} \quad (5)$$

The number 1 in eqs 4 and 5 stands for the electronic charge of $Cu^+$ and $Ag^+$, respectively.

However, for the same temperature,

$$E_{T\,Au} > E_{T\,Cu} \quad (6)$$

$$E_{T\,Au} > E_{T\,Ag} \quad (7)$$

because of the higher oxidation state of $Au^{3+}$.

The diesel soot particles, reacting on the $Au^{3+}$ moieties, may attain the required adsorption activation energy at higher rates than on $Cu^+$ or $Ag^+$, resulting in a higher adsorption rate, which is the determining reaction step for diesel soot oxidation.

## 3. CONCLUSIONS

In summary, the results obtained on the IB group metal-supported ZnO suggest that the diesel soot oxidation activity of metal-supported metal oxide catalysts is determined by the presence of a metal catalytic site involving $M^0-M^{\delta+}$ moieties. Although the $M^0$ moieties accelerate the generation of a superoxide, the $M^{\delta+}$ moieties accelerate the diesel soot adsorption process. The diesel soot adsorption, which is the rate-determining step in diesel soot oxidation process, can be accelerated by increasing its Coulombic potential energy, generated by the Coulombic forces between the $\pi$ electrons of the C=C bonds present in the diesel soot molecules and the ionic metal species $M^{\delta+}$ on the metal NPs. Therefore, the diesel soot oxidation activity of the supported catalysts depends on the number of electric charges of metal ion moieties, which reside at the catalyst surface. We demonstrate the effect of electronic state(s) of metals in metal-supported semiconducting catalysts on their diesel soot oxidation ability. The proposed general model can also be extended to other metal−semiconductor heterogeneous oxidation catalysts. However, we must recognize that the oxidation state of the supported metal over a semiconductor support depends considerably on the process of their fabrication/synthesis.

## 4. EXPERIMENTAL SECTION

**4.1. Catalysts Preparation.** The support used for the preparation of the catalysts was ZnO powder, supplied by Aldrich (99.99%). The catalysts were prepared by impregnation, using the required amounts of aqueous $Cu(NO_3)_2$ (Aldrich 99.99%), $AgNO_3$ (Aldrich 99.99%), and $NaAuCl_4$ (Aldrich 99.99%) solutions to obtain 1 wt % M/ZnO mixtures (M = Cu, Ag, or Au). The suspensions were magnetically stirred at 25 °C for 1 h. The catalysts were recovered by filtration, washed thoroughly to remove unreacted species (soluble sodium and chlorine), and dried under magnetic



DOI: 10.1021/acsomega.8b03142
ACS Omega 2019, 4, 5795−5804

stirring at 120 °C overnight. The resulting powders were reduced under pure $H_2$ at a volume flow rate of 80 mL $min^{-1}$ at 450 °C for 4 h. The temperature of the furnace was increased at the rate of 10 °C $min^{-1}$. The catalysts were cooled down to 25 °C under $H_2$ flow, after which the samples were purged with a nitrogen flow for 30 min. The catalysts were then stored in dry conditions and designated as 1% Cu/ZnO, 1% Ag/ZnO, and 1% Au/ZnO. A ZnO sample was prepared in the same way to use as the reference.

**4.2. Catalyst Characterization.** The $N_2$ adsorption−desorption isotherms of the catalysts were measured using a BELSORP Mini-II (BEL, Japan) sorptometer, after degasification at 400 °C for 2 h. The specific surface area ($S_g$) of the catalysts was determined from their $N_2$ physisorptions at −196 °C, using Brunauer−Emmett−Teller analysis. The isotherms were recorded in the pressure range 0.0−6.6 kPa. The saturation uptake was determined using the technique of back extrapolation of the linear portion of the isotherms to zero equilibrium pressure.

A Shimadzu UV−vis spectrophotometer equipped with an integrating sphere was used to obtain the DRS of the catalysts, using $BaSO_4$ as the standard reflectance sample.

XPS spectra were recorded on freshly prepared 1% Cu/ZnO, 1% Ag/ZnO, and 1% Au/ZnO samples using an ESCALAB 200R electron spectrometer equipped with a hemispherical analyzer, operating in a constant pass energy mode. For recording the XPS spectra of the catalysts, a monochromatic Mg K$\alpha$ emission ($h\nu$ = 1253.6 eV) from the X-ray tube operating at 10 mA and 12 kV was utilized. To get good signal-to-noise ratios, the energy regions of the photoelectrons of interest were scanned a number of times. The intensities of the emission peaks were determined by integrating the area under each peak after subtracting an S-shaped background and fitting the experimental peak to Lorentzian/Gaussian curves (80% L/20% G). Utilizing the position of C 1s signal, coming from adventitious carbon, which appeared around 284.9 ± 0.2 eV, the peak positions of the elements were referenced.

TEM (JEM 2100F microscope fitted with an INCA X-sight, Oxford Instruments), operating at 200 kV accelerating voltage and line resolution of 0.14 nm, was used to characterize the Cu, Ag, and Au particle sizes for each catalyst. Before the TEM analysis, the catalyst samples were ground and suspended in ethanol. A drop of the suspension was then mounted over a carbon-coated copper grid and the solvent was evaporated. The periodic images of the structures on the electron micrographs were analyzed using digital Fourier transformation.

**4.3. Generation of Diesel Soot.** In Figure 11, the schematics of the system used for generating a diesel soot is presented. Pure Mexican diesel was burned in a glass vessel (diesel burner) under an air flow rate of 100 mL $min^{-1}$ for 1 h. In this investigation, for referring both the soluble and insoluble fractions of the diesel emission, the term "diesel soot" is used.

The diesel combustion emission from the exhaust of the vessel was directed to the catalyst sample, which was placed in a tubular quartz reactor with an inner diameter of 1 cm. The reactor was placed in a programmable furnace, as shown in Figure 11. The resulting contact between the diesel soot generated in the glass vessel and the catalyst is considered similar to the contact between the diesel soot generated from a real diesel engine and the catalyzed soot filter. Therefore, the concept of light mode or tight mode contact between the diesel soot and the catalyst used in several research studies cannot be applied here.

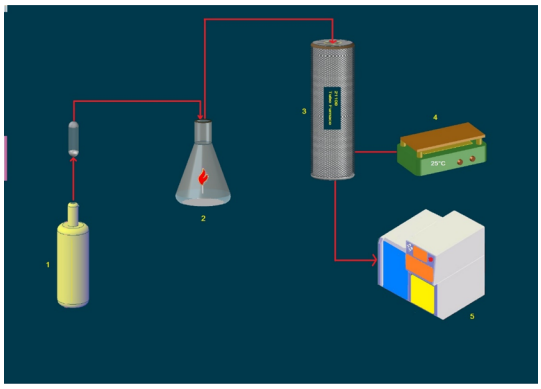


**Figure 11.** Diagram of the system used for studying the generation and catalytic oxidation of diesel soot process. (1) Air; (2) diesel burner; (3) reactor in a programmable furnace; (4) temperature controller; and (5) gas chromatograph.

A Bruker FT-IR spectrometer (Vertex 70) operating in the 800−4000 $cm^{-1}$ spectral range was used for the characterization of the soot generated during diesel combustion in the glass vessel. The diesel combustion emissions were accumulated on ZnO for 1 h under the same conditions. The FT-IR spectrum was recorded using a thin, uniform KBr pellet prepared with 0.2 wt % of the diesel soot/ZnO mixture.

**4.4. Diesel Soot Oxidation through Temperature-Programmed Experiments.** The performance of 1% Cu/ZnO, 1% Ag/ZnO, and 1% Au/ZnO catalysts for diesel soot oxidation was evaluated by temperature-programmed oxidation of the diesel soot/catalyst mixtures. For this purpose, after the diesel soot accumulation over the catalyst, weakly attached combustion products were removed by air (20 vol % of $O_2$ and 80 vol % of $N_2$) flow of 100 mL $min^{-1}$. This flow was maintained during the entire soot oxidation process. The diesel soot/catalyst mixture was then heated from 25 to 600 °C at a heating rate of 5 °C $min^{-1}$.

In order to monitor the reaction temperature along with the exothermic heat of the diesel soot oxidation, a thermocouple was inserted into the diesel soot−catalyst mixture. The diesel soot oxidation products from the reactor were analyzed every 10 min using a Shimadzu gas chromatograph provided with a thermo-conductivity detector to monitor the CO and $CO_2$ evolution at different temperatures. To determine the catalytic effect, diesel soot oxidation was performed under the same conditions using diesel soot/ZnO mixture as the reference at temperatures between 25 and 800 °C.

## ■ ASSOCIATED CONTENT

### Supporting Information

The Supporting Information is available free of charge on the ACS Publications website at DOI: 10.1021/acsomega.8b03142.

High-resolution TEM images of 1% Au/ZnO (PDF)

## ■ AUTHOR INFORMATION

### Corresponding Author

*E-mail: griselda.corro@correo.buap.mx. Phone: +52 22 2295500-7294 (G.C.).



DOI: 10.1021/acsomega.8b03142
ACS Omega 2019, 4, 5795−5804

**ORCID**

Grisel Corro: 0000-0002-7645-4477

Umapada Pal: 0000-0002-5665-106X

**Notes**

The authors declare no competing financial interest.

## ■ ACKNOWLEDGMENTS

The authors acknowledge Vicerrectoria de Investigación y Estudios de Posgrado BUAP (Proyect # 69-2018) and Secretaría de Energía-Consejo Nacional de Ciencia y Tecnología (Cluster Biodiesel Avanzado FSE 250014), Mexico, for their financial support.

## ■ REFERENCES

(1) Bueno-López, A. Diesel soot combustion ceria catalysts. *Appl. Catal., B* **2014**, *146*, 1−11.

(2) Krishna, K.; Bueno-López, A.; Makkee, M.; Moulijn, J. A. Potential rare earth modified $CeO_2$ catalysts for soot oxidation: I. Characterisation and catalytic activity with $O_2$. *Appl. Catal., B* **2007**, *75*, 189−200.

(3) Zokoe, J.; McGinn, P. J. Catalytic diesel soot oxidation by hydrothermally stable glass catalysts. *Chem. Eng. J.* **2015**, *262*, 68−77.

(4) Atribak, I.; Bueno-López, A.; García-García, A. Uncatalysed and catalysed soot combustion under $NO_x$+$O_2$: Real diesel versus model soots. *Combust. Flame* **2010**, *157*, 2086−2094.

(5) Hinot, K.; Burtscher, H.; Weber, A.; Kasper, G. The effect of the contact between platinum and soot particles on the catalytic oxidation of soot deposits on a diesel particle filter. *Appl. Catal., B* **2007**, *71*, 271−278.

(6) Fino, D.; Specchia, V. Open issues in oxidative catalysis for diesel particulate abatement. *Powder Technol.* **2008**, *180*, 64−73.

(7) Lepperhoff, G.; Lüders, H.; Barthe, P.; Lemaire, J. *Quasi-Continuous Particle Trap Regeneration by Cerium-Additives*; SAE International, 1995.

(8) Allansson, R.; Blakeman, P. G.; Cooper, B. J.; Hess, H.; Silcock, P. J.; Walker, A. P. *Optimizing the Low Temperature Performance and Regeneration Efficiency of the Continuously Regenerating Diesel Particulate Filter (CR-DPF) System*; SAE International, 2002.

(9) Setiabudi, A.; van Setten, B. A. A. L.; Makkee, M.; Moulijn, J. A. The influence of $NO_x$ on soot oxidation rate: molten salt versus platinum. *Appl. Catal., B* **2002**, *35*, 159−166.

(10) Reichert, D.; Finke, T.; Atanassova, N.; Bockhorn, H.; Kureti, S. Global kinetic modelling of the reaction of soot with $O_2$ and $NO_x$ on $Fe_2O_3$ catalyst. *Appl. Catal., B* **2008**, *84*, 803−812.

(11) Sun, M.; Wang, L.; Feng, B.; Zhang, Z.; Lu, G.; Guo, Y. The role of potassium in $K/Co_3O_4$ for soot combustion under loose contact. *Catal. Today* **2011**, *175*, 100−105.

(12) Hueso, J.; Caballero, A.; Ocana, M.; Gonzalezelipe, A. Reactivity of lanthanum substituted cobaltites toward carbon particles. *J. Catal.* **2008**, *257*, 334−344.

(13) Atribak, I.; Bueno-López, A.; García-García, A.; Navarro, P.; Frías, D.; Montes, M. Catalytic activity for soot combustion of birnessite and cryptomelane. *Appl. Catal., B* **2010**, *93*, 267−273.

(14) Zouaoui, N.; Issa, M.; Kehrli, D.; Jeguirim, M. $CeO_2$ catalytic activity for soot oxidation under $NO/O_2$ in loose and tight contact. *Catal. Today* **2012**, *189*, 65−69.

(15) Liu, J.; Zhao, Z.; Xu, C.-m.; Duan, A.-j. Simultaneous removal of NOx and diesel soot over nanometer Ln-Na-Cu-O perovskite-like complex oxide catalysts. *Appl. Catal., B* **2008**, *78*, 61−72.

(16) Yamazaki, K.; Sakakibara, Y.; Dong, F.; Shinjoh, H. The remote oxidation of soot separated by ash deposits via silver-ceria composite catalysts. *Appl. Catal., A* **2014**, *476*, 113−120.

(17) Lee, C.; Park, J.-I.; Shul, Y.-G.; Einaga, H.; Teraoka, Y. Ag supported on electrospun macro-structure $CeO_2$ fibrous mats for diesel soot oxidation. *Appl. Catal., B* **2015**, *174*−*175*, 185−192.

(18) Liu, S.; Wu, X.; Liu, W.; Chen, W.; Ran, R.; Li, M.; Weng, D. Soot oxidation over $CeO_2$ and $Ag/CeO_2$: Factors determining the catalyst activity and stability during reaction. *J. Catal.* **2016**, *337*, 188−198.

(19) Corro, G.; Cebada, S.; Pal, U.; Fierro, J. L. G.; Alvarado, J. Hydrogen-reduced Cu/ZnO composite as efficient reusable catalyst for diesel particulate matter oxidation. *Appl. Catal., B* **2015**, *165*, 555−565.

(20) Corro, G.; Vidal, E.; Cebada, S.; Pal, U.; Bañuelos, F.; Vargas, D.; Guilleminot, E. Electronic state of silver in $Ag/SiO_2$ and Ag/ZnO catalysts and its effect on diesel particulate matter oxidation: An XPS study. *Appl. Catal., B* **2017**, *216*, 1−10.

(21) Corro, G.; Cebada, S.; Pal, U.; Fierro, J. L. G. $Au^0$−$Au^{3+}$ bifunctional site mediated enhanced catalytic activity of Au/ZnO composite in diesel particulate matter oxidation. *J. Catal.* **2017**, *347*, 148−156.

(22) Salamanca, M.; Mondragón, F.; Agudelo, J. R.; Benjumea, P.; Santamaría, A. Variations in the chemical composition and morphology of soot induced by the unsaturation degree of biodiesel and a biodiesel blend. *Combust. Flame* **2012**, *159*, 1100−1108.

(23) Bellamy, L. J. *The Infrared Spectra of Complex Molecules*, 3rd ed.; Chapman and Hall Ltd.: London, 1975.

(24) Sarbak, Z. Characterization and infrared study of the effect of Cr, Mo and W on carbon deposition on platinum/alumina. *Appl. Catal., A* **1999**, *177*, 85−97.

(25) Ozin, G. A.; Huber, H. Cryophotoclustering techniques for synthesizing very small, naked silver clusters $Ag_n$ of known size (where n = 2-5). The molecular metal cluster-bulk metal particle interface. *Inorg. Chem.* **1978**, *17*, 155−163.

(26) McIntosh, D.; Ozin, G. A. Synthesis using metal vapors. Silver carbonyls. Matrix infrared, ultraviolet-visible, and electron spin resonance spectra, structures, and bonding of silver tricarbonyl, silver dicarbonyl, silver monocarbonyl, and disilver hexacarbonyl. *J. Am. Chem. Soc.* **1976**, *98*, 3167−3175.

(27) Kowalska, E.; Mahaney, O. O. P.; Abe, R.; Ohtani, B. Visible-light-induced photocatalysis through surface plasmon excitation of gold on titania surfaces. *Phys. Chem. Chem. Phys.* **2010**, *12*, 2344−2355.

(28) Tan, Z. Y.; Yong, D. W. Y.; Zhang, Z.; Low, H. Y.; Chen, L.; Chin, W. S. Nanostructured Cu/ZnO Coupled Composites: Toward tunable Cu nanoparticle sizes and plasmon absorption. *J. Phys. Chem. C* **2013**, *117*, 10780−10787.

(29) Hu, Y.; Chen, H.-J. Preparation and characterization of nanocrystalline ZnO particles from a hydrothermal process. *J. Nanopart. Res.* **2007**, *10*, 401−407.

(30) Linnert, T.; Mulvaney, P.; Henglein, A.; Weller, H. Long-lived nonmetallic silver clusters in aqueous solution: preparation and photolysis. *J. Am. Chem. Soc.* **1990**, *112*, 4657−4664.

(31) Ershov, B. G.; Janata, E.; Michaelis, M.; Henglein, A. Reduction of aqueous copper(2+) by carbon dioxide(1-): first steps and the formation of colloidal copper. *J. Phys. Chem.* **1991**, *95*, 8996−8999.

(32) Grundmann, M. *The Physics of Semiconductors*, 3rd ed.; Springer International Publishing: New York, 2016; Vol. 3, pp XXXIX−989.

(33) Singh, S. C.; Gopal, R. Zinc nanoparticles in solution by laser ablation technique. *Bull. Mater. Sci.* **2007**, *30*, 291−293.

(34) Richter, M.; Langpape, M.; Kolf, S.; Grubert, G.; Eckelt, R.; Radnik, J.; Schneider, M.; Pohl, M. M.; Fricke, R. Combinatorial preparation and high-throughput catalytic tests of multi-component $deNO_x$ catalysts. *Appl. Catal., B* **2002**, *36*, 261−277.

(35) Hoflund, G. B.; Hazos, Z. F.; Salaita, G. N. Surface characterization study of Ag, AgO, and $Ag_2O$ using x-ray photo-electron spectroscopy and electron energy-loss spectroscopy. *Phys. Rev. B: Condens. Matter Mater. Phys.* **2000**, *62*, 11126−11133.

(36) She, X.; Flytzanistephanopoulos, M. The role of AgOAl species in silver-alumina catalysts for the selective catalytic reduction of $NO_x$ with methane. *J. Catal.* **2006**, *237*, 79−93.

(37) Lu, W.; Gao, S.; Wang, J. One-Pot Synthesis of Ag/ZnO self-assembled 3D hollow microspheres with enhanced photocatalytic performance. *J. Phys. Chem. C* **2008**, *112*, 16792−16800.



DOI: 10.1021/acsomega.8b03142
*ACS Omega* 2019, 4, 5795−5804

(38) Balachandran, S.; Selvam, K.; Babu, B.; Swaminathan, M. The simple hydrothermal synthesis of Ag−ZnO−$SnO_2$ nanochain and its multiple applications. *Dalton Trans.* **2013**, *42*, 16365−16374.
(39) Fein, D.; Wachs, I. E. Quantitative determination of the catalytic activity of bulk metal oxides for formic acid oxidation. *J. Catal.* **2002**, *210*, 241−254.
(40) Lin, D.; Wu, H.; Zhang, R.; Pan, W. Enhanced Photocatalysis of Electrospun Ag−ZnO Heterostructured Nanofibers. *Chem. Mater.* **2009**, *21*, 3479−3484.
(41) Han, Z.; Ren, L.; Cui, Z.; Chen, C.; Pan, H.; Chen, J. Ag/ZnO flower heterostructures as a visible-light driven photocatalyst via surface plasmon resonance. *Appl. Catal., B* **2012**, *126*, 298−305.
(42) Villani, K.; Brosius, R.; Martens, J. Catalytic carbon oxidation over Ag/Al2O3. *J. Catal.* **2005**, *236*, 172−175.
(43) Aneggi, E.; Llorca, J.; de Leitenburg, C.; Dolcetti, G.; Trovarelli, A. Soot combustion over silver-supported catalysts. *Appl. Catal., B* **2009**, *91*, 489−498.
(44) Guzman, J.; Carrettin, S.; Fierro-Gonzalez, J. C.; Hao, Y.; Gates, B. C.; Corma, A. CO oxidation catalyzed by supported gold: cooperation between gold and nanocrystalline rare-earth supports forms reactive surface superoxide and peroxide species. *Angew. Chem., Int. Ed.* **2005**, *44*, 4778−4781.
(45) Wei, Y.; Zhao, Z.; Liu, J.; Liu, S.; Xu, C.; Duan, A.; Jiang, G. Multifunctional catalysts of three-dimensionally ordered macroporous oxide-supported Au@Pt core-shell nanoparticles with high catalytic activity and stability for soot oxidation. *J. Catal.* **2014**, *317*, 62−74.
(46) Silva, C. G.; Sampaio, M. J.; Carabineiro, S. A. C.; Oliveira, J. W. L.; Baptista, D. L.; Bacsa, R.; Machado, B. F.; Serp, P.; Figueiredo, J. L.; Silva, A. M. T.; Faria, J. L. Developing highly active photocatalysts: Gold-loaded ZnO for solar phenol oxidation. *J. Catal.* **2014**, *316*, 182−190.
(47) Liu, X.; Liu, M.-H.; Luo, Y.-C.; Mou, C.-Y.; Lin, S. D.; Cheng, H.; Chen, J.-M.; Lee, J.-F.; Lin, T.-S. Strong Metal-Support Interactions between Gold Nanoparticles and ZnO Nanorods in CO Oxidation. *J. Am. Chem. Soc.* **2012**, *134*, 10251−10258.



DOI: 10.1021/acsomega.8b03142
*ACS Omega* 2019, 4, 5795−5804